Measurement and analysis of phased array data on haystacked tones from a source located in a free jet

Tester, Brian J.; Sijtsma, Pieter

DOI
10.2514/6.2017-3864

Publication date
2017

Document Version
Accepted author manuscript

Published in
23rd AIAA/CEAS Aeroacoustics Conference

Citation (APA)
Tester, B. J., & Sijtsma, P. (2017). Measurement and analysis of phased array data on haystacked tones from a source located in a free jet. In *23rd AIAA/CEAS Aeroacoustics Conference: 5-9 June 2017, Denver, Colorado* Article AIAA 2017-3864 American Institute of Aeronautics and Astronautics Inc. (AIAA). https://doi.org/10.2514/6.2017-3864

This is an Accepted Manuscript of a paper published in:
23rd AIAA/CEAS Aeroacoustics Conference, 5-9 June 2017, Denver, Colorado
Available online: https://doi.org/ 10.2514/6.2017-3864

Measurement and analysis of phased array data on haystacked tones from a source located in a free jet

Brian J. Tester*
University of Southampton, Highfield, Southampton, SO17 1BJ, UK

Pieter Sijtsma †
PSA3, 8091 AV Wezep, The Netherlands

Significant spectral broadening of tone noise by jet shear-layer turbulence can occur if the tone frequency and the path length through the shear layer are sufficiently large. A typical example of spectral broadening or 'tone haystacking' are turbine aero-engine tones which exhibit little or no haystacking when measured inside the engine but are sometimes so strongly haystacked in the far-field that the original tone cannot be observed in the measured spectrum. This haystacking of turbine tones requires an engineering method that can predict both the far-field haystacking and the associated reduction in incident tone level. A previous published method, the so-called 'beta' correlation has displayed encouraging agreement with a number of experimental datasets but significant disagreement with others. In this paper another set of experimental data, which includes phased array data, is analysed. The objective is to improve our understanding of the tone haystacking mechanisms with the aid of beamforming and to compare with a prediction from weak scattering theory, in the form of a simple Doppler shift relationship between frequency and angle scattering, assuming a frozen turbulence model. The experimental data acquired by QinetiQ and CLEAN-SC beamformer results described herein begin to provide validation of that prediction, which may lead to resolution of the discrepancies previously observed between the beta correlation and the data acquired under a GARTEUR project.

Nomenclature

M_c	Mach number of turbulence convection speed	r	radial co-ordinate
M_T	Mach number of free-jet mean exit velocity	θ	polar angle of incident tone radiation, relative to downstream jet axis
V_c	turbulence convection speed		
V_T	free-jet mean exit velocity	Θ	polar angle of scattered tone radiation, relative to downstream jet axis
a_0	ambient sound speed		
d	free-jet nozzle diameter	ω	radian frequency of incident tone
x	axial co-ordinate	Ω	radian frequency of scattered wave

I. Introduction

SIGNIFICANT spectral broadening of tone noise by jet shear layer turbulence can occur if the tone frequency and the path length through the shear layer are sufficiently large. Typical examples of spectral broadening or 'tone haystacking' are turbine aero-engine tones, see Figure 1, which exhibit little or no haystacking when measured inside the engine but are sometimes so strongly haystacking in the far-field that the original tone cannot be detected in the measured spectra. Another example can be seen in the tones generated by model turbomachinery rigs when mounted inside a free-jet wind tunnel such as the Large Low-speed Facility (LLF) of DNW.

---

* Principal Research Fellow, ISVR, Faculty of Engineering and the Environment; AIAA Senior member
† Director; also at Aircraft Noise & Climate Effects, Delft University of Technology, Faculty of Aerospace Engineering, The Netherlands

As a result of a recent European collaborative project GARTEUR AD/AG-50: "Effect of Open Jet Shear Layers on Aeroacoustic Wind Tunnel Measurements", a number of experimental investigations into tone haystacking were conducted by the partners, which were summarised by Sijtsma et al.[1]. A similar investigation, within the same GARTEUR group, was carried out by Kröber et al.[2]. Some of these datasets were shown to agree reasonably well with a simple theoretical model, which predicts the characteristics of spectral broadening in terms of time delay variations. The spectral broadening was assumed to be caused by random variations in the propagation time between source and microphone, the time delay variations being due to the turbulence in the shear layer. Applying several assumptions and simplifications, a simple physical model was obtained which predicted the amount of broadening (loss of acoustic energy in a tone) as a function of a few experimental parameters. A broadening parameter, β, was defined which is proportional to wind speed, source frequency and shear layer thickness. Their conclusions were as follows.

For the DNW-PLST, the DNW-NWB and the VKI wind tunnels, the agreement between prediction and experiment was good. For a complete range of wind speeds, source frequencies and axial source positions, the amount of broadening (i.e., the energy ratio) only depended on the value of the broadening parameter, which made it possible to retrieve the original level of a tone from a broadened spectrum, as long as the tone could be identified.

In the case of the DNW-LLF wind tunnel, the agreement between experiment and prediction method was less good. The shear layer was much thicker than in the other tunnels, and as a result more broadening occurred and at high frequencies the tone could not be clearly identified. For the cases where a tone could be identified, there was no unequivocal relation between the energy ratio and β. Thus, the applicability of the present prediction method to retrieve original tone levels in the DNW-LLF appeared to be limited.

For the NLR-KAT wind tunnel, an unequivocal relationship was found between β and the energy ratio for the complete range of wind speeds and source frequencies, which offered the possibility of retrieving the original tone level from the broadened spectrum. However, the relationship between β and energy ratio was found to depend on the source position, which limits the applicability of the prediction method for this tunnel.

It was concluded that for these two wind tunnels, the discrepancies are probably caused by some violation of the theoretical scaling assumptions and associated simplifications.

In the current paper, we investigate another set of experimental data, which was acquired in the QinetiQ Noise Test Facility by M. Harper-Bourne, also as part of the GARTEUR project, and which included a phased polar array. The objective was to improve our understanding of the tone haystacking mechanisms with the aid of beamforming and the weak scattering theory proposed by Cargill[3], as extended by Powles et al.[4] and McAlpine et al.[5]. Part II describes that experiment, Part III presents an analysis of the far-field and the beamformer data and Part IV describes a comparison of one aspect of the Cargill theory with the observations extracted from the processed beamformer data.

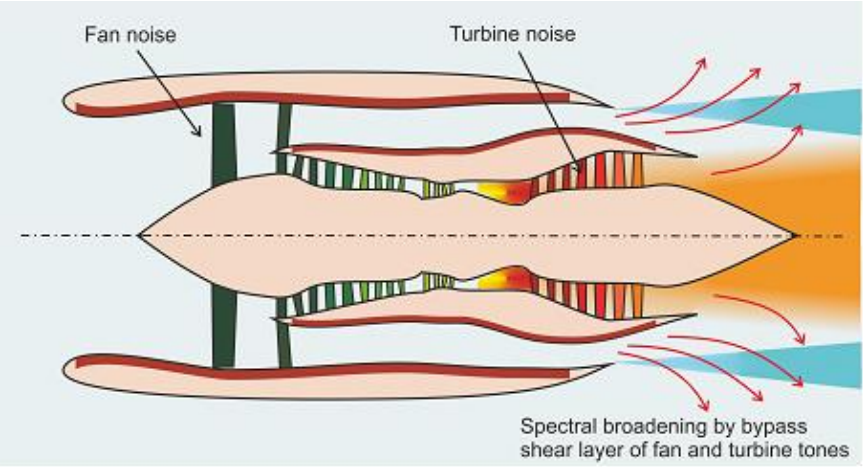

Figure 1: Haystacking of turbine tones by bypass shear layer (fan tones can also be haystacked but less strongly)

II. Description of Experiment

A set of tone haystacking experimental data was acquired in the QinetiQ Noise Test Facility by M. Harper-Bourne in 2009 using a free-jet/source configuration depicted in Figure 2. A far-field array was located on a polar radius of 12 m centred on the source covering a polar angle range from 30° to 120° to the downstream jet axis, in steps of 10°, see Figure 3. A phased polar array of 95 electret microphones was deployed at a polar radius of 11.4 m centred on the source, with an aperture spanning 90° to 30°, see Figure 4.

The objective of the experiment was first to acquire a tone haystacking dataset with a realistic circular jet nozzle (diameter of 1.8m) and jet shear layer over a range of frequencies and jet Mach numbers that would enable us to observe the transition from weak to strong scattering, a topic that will be addressed in a future paper. Here the main objective is to use the polar phased array data to improve our understanding of the tone haystacking mechanisms and to compare results with some aspects of the weak scattering theory.

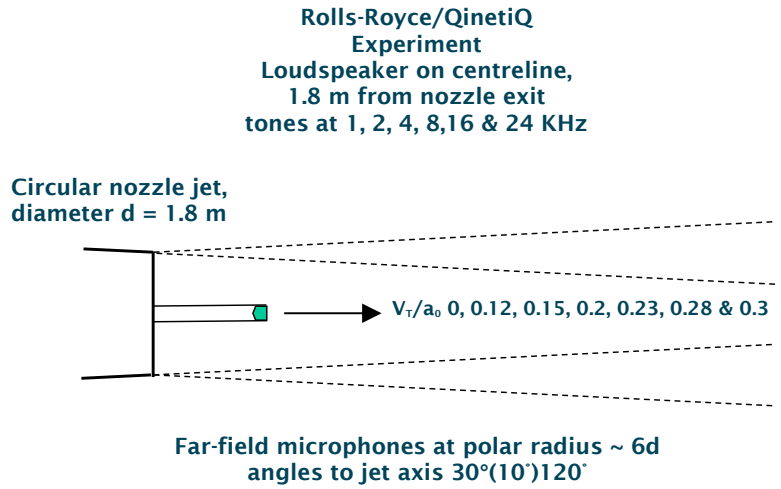

Figure 2: The free jet with loudspeaker source mounted on a test nozzle

Figure 3: The free-jet, jet nozzle and far-field microphones in the QinetiQ Noise Test Facility

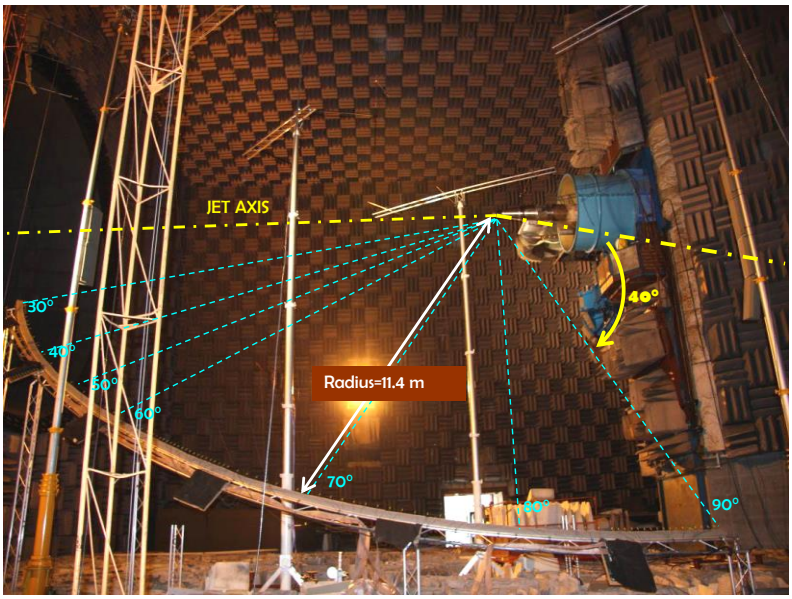

Figure 4: The polar phased array

III. Analysis of far-field and beamformer data

A. Far-field data

Typical far-field data are shown in Figure 5 for a range of incident frequencies for Mach 0.15. At the lower frequencies (1, 2, 4 kHz) we see similar spectral shapes, featuring a peak at the incident frequency and haystacked 'humps' at neighbouring frequencies. The peaks are pure tones and the side humps contain broadband noise. At these lower incident frequencies the haystacking is called "weak". With increasing frequency the contribution of the pure incident tone becomes smaller and smaller, until it disappears at around 8 kHz. At higher frequencies the haystacking is called "strong".

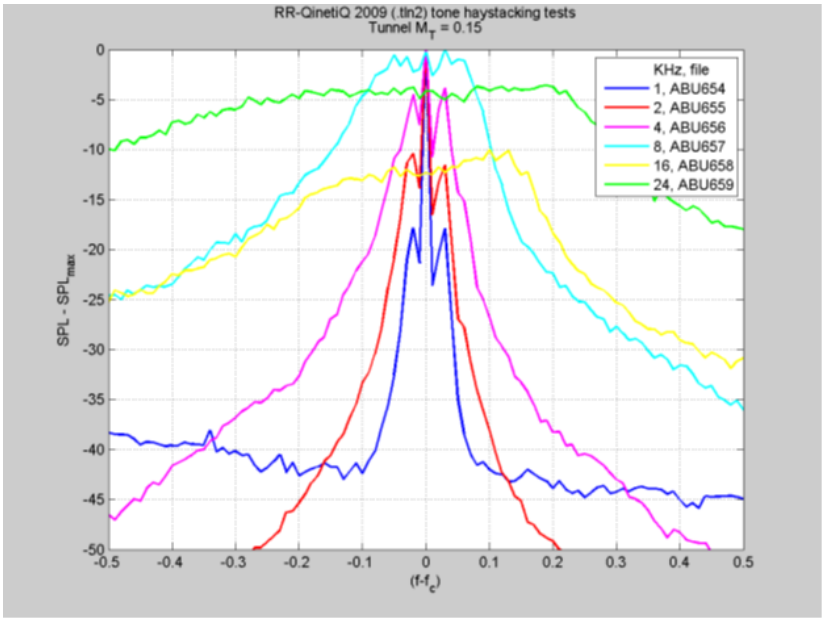

Figure 5: Typical weak to strong haystacked spectra, at 90°, free-jet Mach = 0.15, tone frequencies 1-24 kHz; far-field array, 10 Hz filter separation

B. Polar array beamformer data

In order to investigate, by beamforming, haystacking phenomena at different radiation angles, the polar array was divided into 4 sectors, as depicted in Figure 6. The non-equidistant spacing of the microphones was counterbalanced by giving each microphone an appropriate weight in the beamforming process. The weighted average microphone positions in each sector, which are depicted by the black crosses, will act as reference positions in the analysis to follow. Their respective angular positions with respect to the downstream jet axis are 82.4°, 67.6°, 52.1° and 37.9°.

Conventional delay-and-sum beamformer images at 1 and 2 kHz of Sector 1 are shown in Figure 7. Beamforming was done without correction for flow, so the source is expected to be found at a position shifted downstream from the true source position, which is at axial location $x = 0.18$ m ($x = 0$ m being the centre of the polar arc). In this case the expected downstream shift is 14 cm, so the apparent source is expected to be at $x = 0.32$ m. This is indeed, more or less, where the peak at the incident tone frequency appears to be. However, the haystack 'humps' at about 985 Hz and 1015 are shifted relative to that downstream and upstream respectively.

The axial resolution in Figure 7 is quite poor. This is the penalty of using a "sector" array covering a small range of angles. From these images it is therefore not clear if there is just one single source direction, or if several incoherent source directions exist. To investigate this, CLEAN-SC[6] was applied. The "loop gain" factor was set to 0.1.

The CLEAN-SC counterpart of Figure 7 is shown in Figure 8. The image at 1 kHz shows, within the 40 dB plot range, one single source per frequency bin. The 2 kHz image shows a few low-level sources from other directions. These images suggest a simple relationship between apparent source variation and frequency shift. The peak locations found with CLEAN-SC will be compared to a prediction from weak scattering theory in the next section.

CLEAN-SC results with the other array sectors are shown in Figure 9 to Figure 11. With decreasing sector angle, we can see an increasing variation in apparent source position. Generally, a single dominant source direction exists at each frequency. It is interesting to note that "side lines" appear at the 2 kHz images. Nevertheless, for the comparison with theory in the next section we will only use the peak directions.

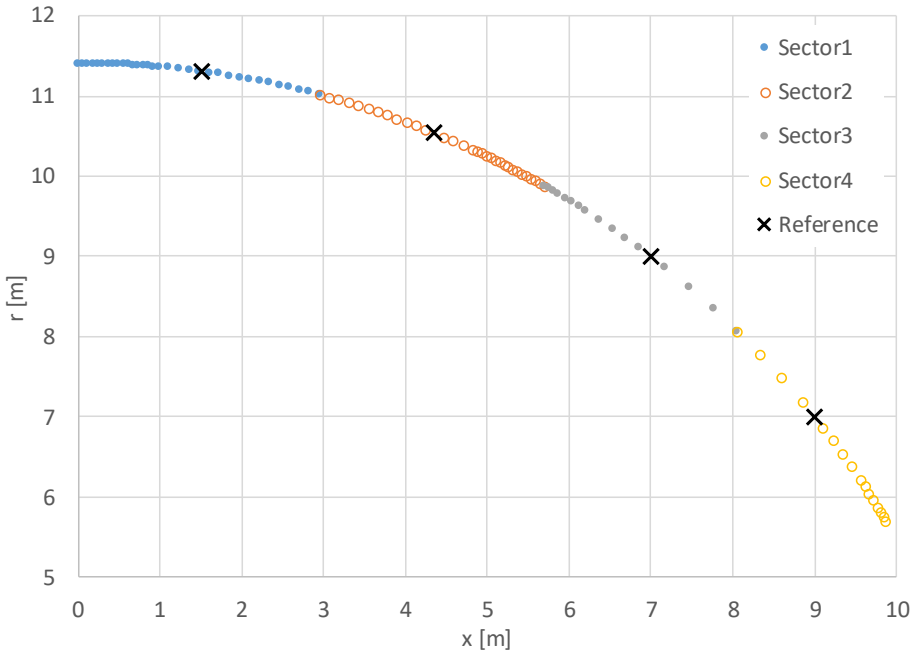

Figure 6: Polar array sectors, with reference microphone positions at 82.4°, 67.6°, 52.1° and 37.9°

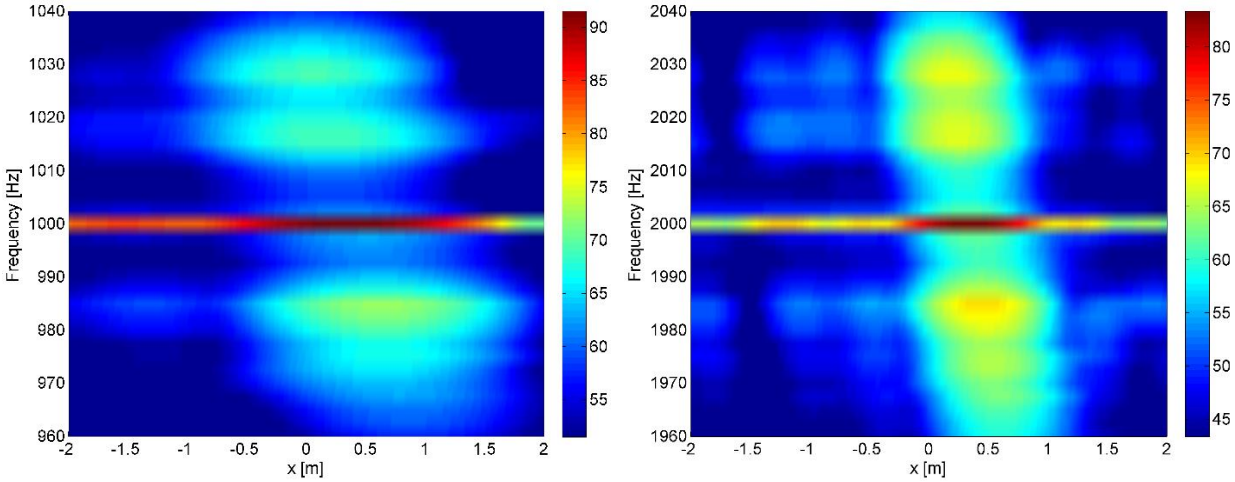

Figure 7: Conventional beamformer images, Mach = 0.15, Sector 1 (82.4°);
Left: 1 kHz incident frequency, Right: 2 kHz incident frequency

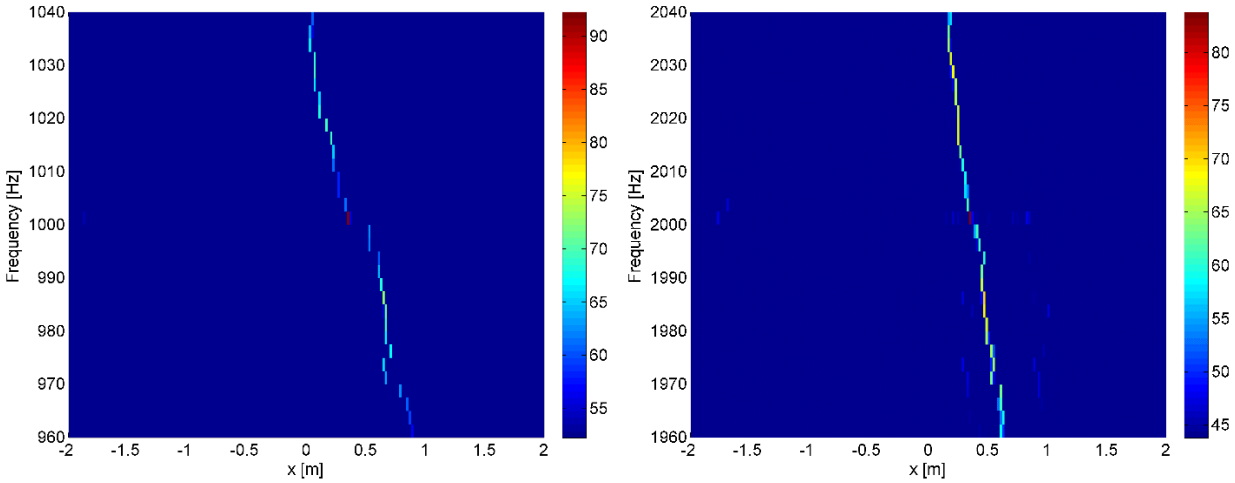

Figure 8: CLEAN-SC beamformer image, Mach = 0.15, Sector 1 (82.4°);
Left: 1 kHz incident frequency, Right: 2 kHz incident frequency

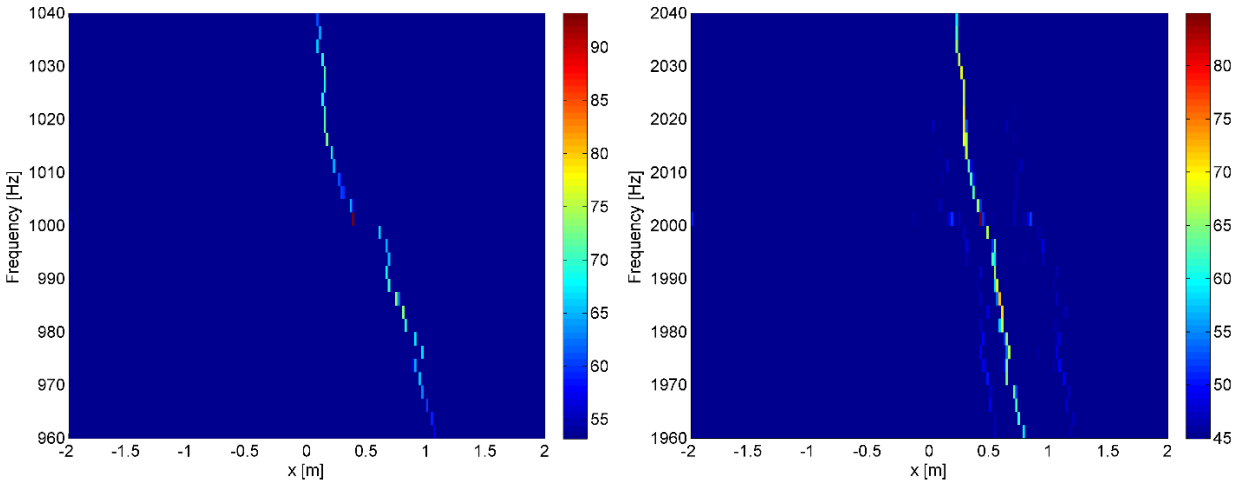

Figure 9: CLEAN-SC beamformer image, Mach = 0.15, Sector 2 (67.6°);
Left: 1 kHz incident frequency, Right: 2 kHz incident frequency

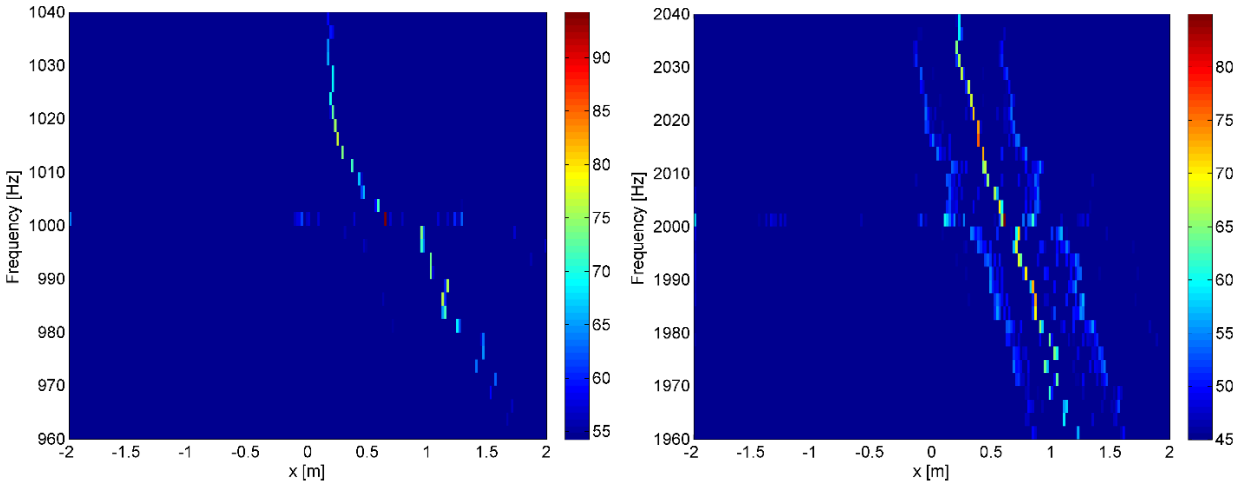

Figure 10: CLEAN-SC beamformer image, Mach = 0.15, Sector 3 (52.1°);
Left: 1 kHz incident frequency, Right: 2 kHz incident frequency

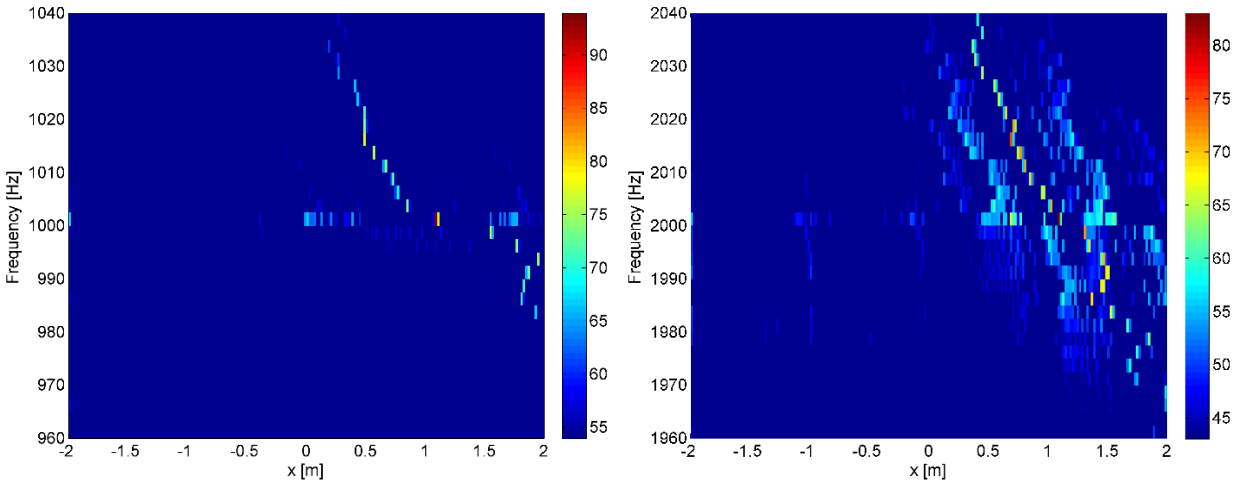

Figure 11: CLEAN-SC beamformer image, Mach = 0.15, Sector 4 (37.9°);
Left: 1 kHz incident frequency, Right: 2 kHz incident frequency

IV. Comparison of experimental beamformer results with weak scattering theory

The apparent shift of source position at the *incident* frequency from the CLEAN-SC images varies with the angle of observation as expected, see Figure 12, which can be predicted using Snell's Law, as illustrated in Figure 13. In other words, the peak locations obtained with the CLEAN-SC beamformer agree well with that calculated by Snell's Law. A summary of the essentials of Snell's Law can be found in the Appendix.

The apparent shift of source position at the scattered frequencies has not been investigated in detail before and is compared here with that obtained from the weak scattering relationship derived by Cargill, as noted by Powles et al.[4]. The incident sound wave at frequency, ω, radiated from the shear layer at angle, θ, at the far-field microphone, is accompanied by a range of scattered waves, frequency, Ω, radiated at a different angle, Θ, which are related by the weak scattering relationship, assuming a 'frozen turbulence' model, by

$$\Omega\left(1-M_c\cos\Theta\right)=\omega\left(1-M_c\cos\theta\right), \tag{1}$$

where M_c is the turbulence convection Mach number. Note that this equality has been applied below to radiation from the same point in the shear layer, so in Figure 13 it applies to the red symbols Θ and $\tilde{\theta}$. However, Eq. 1 was derived by Cargill in terms of angular relationships in the far-field, where $\tilde{\theta}\to\theta$; here the observer microphone is

in the geometric near field, which is being modelled with ray paths and hence the distinction between the incident and scattered ray paths.

In the Appendix the same relationship is derived in an alternative way, based on Doppler frequency shift due to the time-dependency of the acoustic path length. An equivalent relation was also derived by Schlinker and Amiet[7].

A curve that shows, at a given microphone angular position, the relation between shifted frequency and shifted apparent source position can be constructed as follows. Start from a set of apparent source positions in a range of, say, ± 1 m around the apparent source position predicted by Snell's Law (and depicted in Figure 12). For each of these apparent source positions, the shifted frequency is determined through the following steps:

a) The scatter angle Θ and the shear layer intersection point follow directly from the line of sight between the apparent source and the microphone (see Figure 13).
b) The standard radiation angle $\tilde{\theta}$ follows from Snell's Law, Eq. (10) in the Appendix, knowing also the true source position.
c) The normalised frequency shift, $\Omega/\omega - 1$, is then calculated from the weak scattering relationship, Eq. (1).

The thus constructed curves, at the four reference sector angles, are shown in Figure 14 and Figure 15, and compared with the CLEAN-SC peak locations.

Figure 14 shows the results for the first two polar array sectors (82.4° and 67.6°), where the agreement between predictions and measurements is good. Less good agreement is found for Sector 3 (52.1°) and Sector 4 (37.9°), as depicted in Figure 15. At the lowest sector angle, the slope of the measured data is less steep than predicted. This can be explained by the strong angular dependence (directivity) of the tones in Sector 4. Below 35° the measured tone levels decay quickly, so the effective centre of Sector 4 is localised at a sector angle greater than 37.9°.

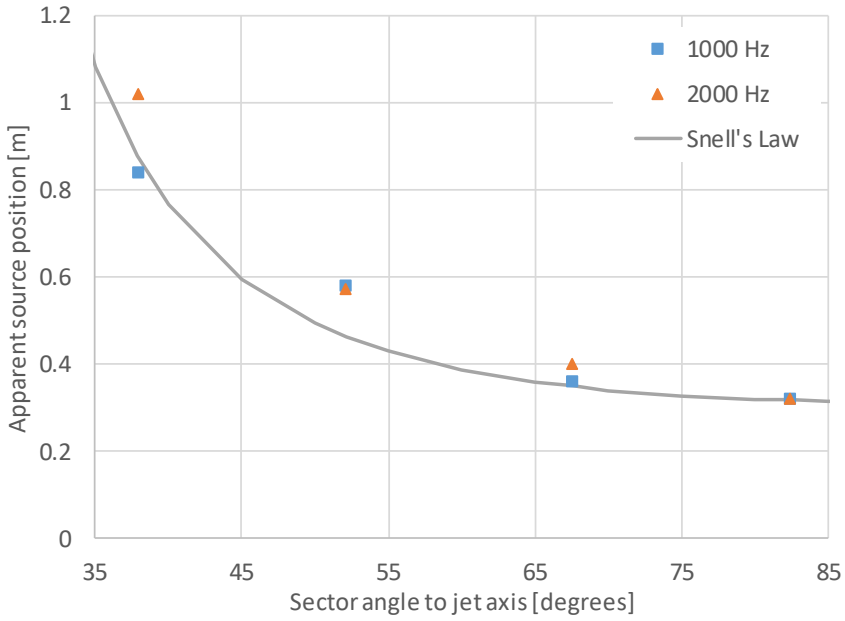

Figure 12: Apparent shift of source position at *incident* frequency, CLEAN-SC beamformer data (symbols) compared to Snell's Law (line), Mach = 0.15.

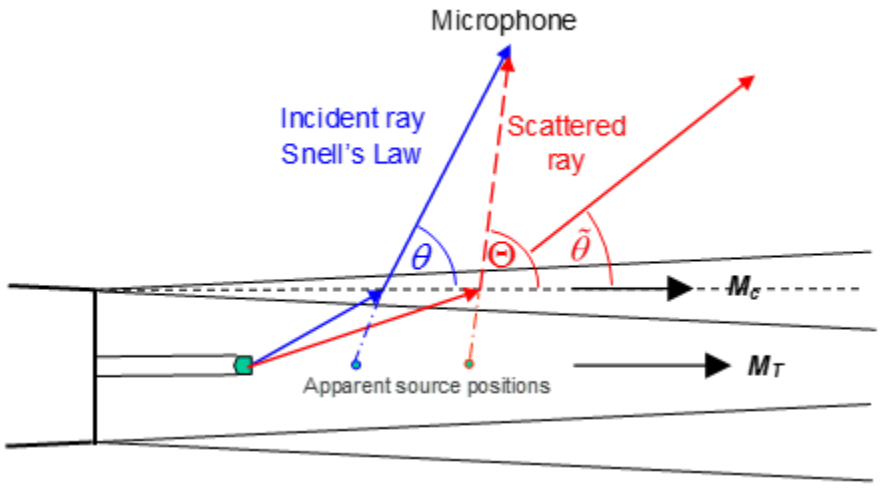

Figure 13: Refraction (blue) and scatter (red) of acoustic wave through the jet shear layer

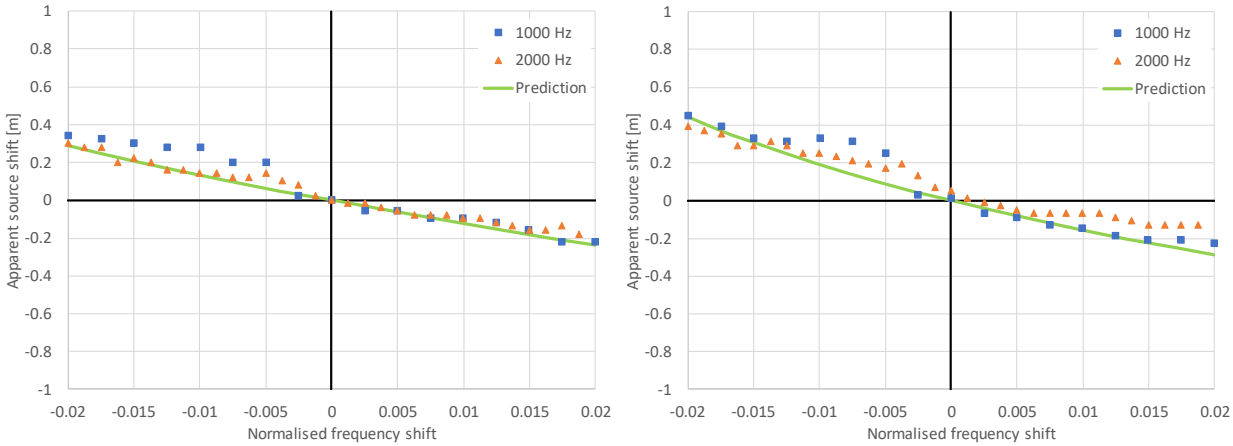

Figure 14: Shift of apparent source position with *scattered* frequency, CLEAN-SC beamformer data (symbols) compared to weak scattering prediction (line), Mach = 0.15;
Left: Sector 1 (82.4°), Right: Sector 2 (67.6°)

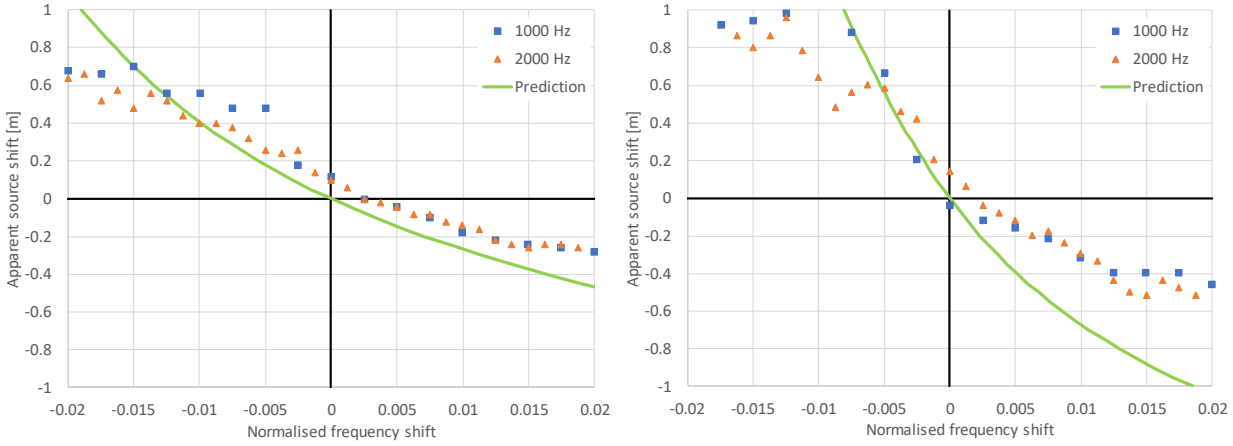

Figure 15: Shift of apparent source position with *scattered* frequency, CLEAN-SC beamformer data (symbols) compared to weak scattering prediction (line), Mach = 0.15;
Left: Sector 3 (52.1°), Right: Sector 4 (37.9°)

V. Conclusions

The haystacking of turbine tones requires an engineering method, like the previously published β-correlation, which can predict the far-field spectral broadening or 'tone haystacking' and the associated reduction in incident tone level. The Cargill weak scattering model could provide results to benchmark such a method but the Cargill model itself requires validation.

The QinetiQ database and CLEAN-SC beamformer results described herein begin to provide such a validation and may help to resolve the discrepancies previously observed between the beta correlation and the data acquired under the GARTEUR project.

Acknowledgments

The authors are grateful to the UK Government for supporting the SYMPHONY program during which the model-scale data was acquired in the QinetiQ NTF by M. Harper-Bourne, whose efforts are warmly acknowledged. The lead author is grateful to Rolls-Royce and to EPSRC (UK) for financial support.

Appendix: Analysis details

This appendix provides some details for a better understanding of refraction by a shear layer and the frequency/angle scattering induced by the convected turbulence.

A. Standard shear layer refraction

Consider a source on the jet axis $r = r_0$ at axial position $x = \xi$. Let $r = r_s$ describe the shear layer and (x, r) an out-of-flow receiver location, see Figure 16. The shear layer induces refraction of the acoustic ray, so that the 'apparent source', seen from the receiver, moves downstream to (ξ_a, r_0). The acoustic path intersects the shear layer in (x_s, r_s). The sound speed a_0 is assumed to be equal on both sides of the shear layer.

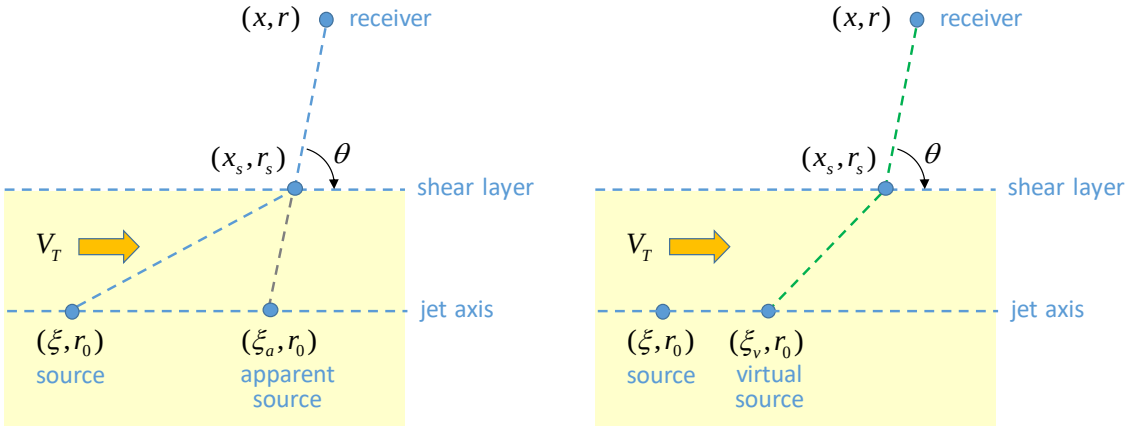

Figure 16: Shear layer refraction sketches

The axial co-ordinate x_s of the shear layer intersection point can be determined by minimising the acoustic time delay between source and receiver. The time delay Δt is a summation of the in-flow time delay Δt_{in} between source and shear layer, and the out-of-flow part Δt_{out}. The latter is calculated by

$$\Delta t_{\text{out}} = \frac{1}{a_0}\sqrt{(x - x_s)^2 + (r - r_s)^2}\,. \tag{2}$$

Likewise, the in-flow part is

$$\Delta t_{\text{in}} = \frac{1}{a_0}\sqrt{(x_s-\xi_v)^2+(r_s-r_0)^2}\ , \tag{3}$$

where ξ_v is the axial co-ordinate of the 'virtual' (or convected) source:

$$\xi_v = \xi + V_T \Delta t_{\text{in}}\ . \tag{4}$$

From Eqs. (3) and (4) we derive

$$\Delta t_{\text{in}} = \frac{1}{\mu^2 a_0}\left[-M_T(x_s-\xi)+\sqrt{(x_s-\xi)^2+\mu^2(r_s-r_0)^2}\right], \tag{5}$$

where

$$M_T = \frac{V_T}{a_0},\ \mu^2 = 1-M_T^2\ . \tag{6}$$

To determine the shear layer intersection point, the total time delay, (5) + (2), is differentiated with respect to x_s and set to zero. The result is essentially Snell's Law:

$$\frac{x-x_s}{\sqrt{(x-x_s)^2+(r-r_s)^2}} = \frac{1}{\mu^2}\left[-M_T+\frac{x_s-\xi}{\sqrt{(x_s-\xi)^2+\mu^2(r_s-r_0)^2}}\right], \tag{7}$$

which needs to be solved numerically for x_s. The left-hand side of Eq. (7) is the cosine of the out-of-flow radiation angle θ (see Figure 13):

$$\cos\theta = \frac{1}{\mu^2}\left[-M_T+\frac{x_s-\xi}{\sqrt{(x_s-\xi)^2+\mu^2(r_s-r_0)^2}}\right]. \tag{8}$$

B. Frequency/angle scattering

Consider a microphone at (x_m, r_m). The shear layer interaction point that fixes the path between the out-of-flow microphone and the in-flow source is obtained by replacing (x,r) by (x_m, r_m) in Eq. (7) and solving it for x_s. This path is indicated in blue in Figure 13. The out-of-flow radiation direction then satisfies Eq. (8).

However, because of the turbulence in the shear layer, sound can also reach the microphone from other directions, say with radiation angle Θ. Sound can be bounced, as it were, by moving eddies (assuming frozen turbulence) in the shear layer (see red dashed line in Figure 13). The shifted shear layer location $\tilde{x}_s$ at which the sound "bounces" is given by

$$\tilde{x}_s = x_m - \cot\Theta\left(r_m - r_s\right). \tag{9}$$

Normally, the direction of sound that radiates from the shifted shear layer location follows from Eq. (8):

$$\cos\tilde{\theta} = \frac{1}{\mu^2}\left[-M_T+\frac{\tilde{x}_s-\xi}{\sqrt{(\tilde{x}_s-\xi)^2+\mu^2(r_s-r_0)^2}}\right]. \tag{10}$$

The shifted shear layer location $\tilde{x}_s$ is associated with a turbulent eddy, moving at convection speed $V_c = 0.5V_T$. Therefore, the path length, and thus the time delay, varies with time. Consequently, the measured frequencies will be Doppler-shifted compared to the emitted frequency. The Doppler shift can be obtained as follows.

A signal with varying frequency can be written as $s(t) = \exp\left(ig(t)\right)$, where the derivative $g'(t)$ is the time-dependent angular frequency ω. This can be understood by writing, for small values of $\tau - t$,

$$s(\tau) = s(t)\exp\left[i\left(g(\tau)-g(t)\right)\right] \approx s(t)\exp\left(i(\tau-t)g'(t)\right). \tag{11}$$

The frequency of a signal with a time-dependent delay Δt is Doppler-shifted:

$$\frac{d}{dt}g(t-\Delta t) = g'(t-\Delta t)\left(1-\frac{d\Delta t}{dt}\right). \tag{12}$$

If the emitted signal has constant frequency, $g(t) = \omega t$, and if we use the symbol Ω for the Doppler-shifted frequency, we have

$$\frac{\Omega}{\omega} = 1 - \frac{d\Delta t}{dt} \quad . \tag{13}$$

Herein we have

$$\Delta t = \Delta t_{\text{in}} + \Delta t_{\text{out}} , \tag{14}$$

where the right-hand side terms are given by Eqs. (5) and (2), replacing x_s by $\tilde{x}_s$.

The shear layer intersection point follows the motion of a turbulent eddy, say $x = x_e(t) = V_c t$, but its time-dependency must be corrected for the time delay with the microphone:

$$\tilde{x}_s = V_c \left(t - \Delta t_{\text{out}} \right). \tag{15}$$

With this we write

$$\frac{d\Delta t_{\text{out}}}{dt} = \frac{d\Delta t_{\text{out}}}{d\tilde{x}_s} \frac{d\tilde{x}_s}{dt} = -M_c \cos\Theta \left(1 - \frac{d\Delta t_{\text{out}}}{dt} \right), \tag{16}$$

with $M_c = V_c / a_0$. From Eq. (16) we derive:

$$\frac{d\Delta t_{\text{out}}}{dt} = \frac{-M_c \cos\Theta}{1 - M_c \cos\Theta} . \tag{17}$$

For the inflow part of the time delay we have, with Eq. (10),

$$\frac{d\Delta t_{\text{in}}}{dt} = \frac{d\Delta t_{\text{in}}}{d\tilde{x}_s} \frac{d\tilde{x}_s}{dt} = M_c \cos\tilde{\theta} \left(1 - \frac{d\Delta t_{\text{out}}}{dt} \right) = \frac{M_c \cos\tilde{\theta}}{1 - M_c \cos\Theta} . \tag{18}$$

Thus, for Eq. (13) we get

$$\frac{\Omega}{\omega} = 1 - \frac{d\Delta t_{\text{in}}}{dt} - \frac{d\Delta t_{\text{out}}}{dt} = \frac{1 - M_c \cos\tilde{\theta}}{1 - M_c \cos\Theta} , \tag{19}$$

which is the same as Cargill's expression, Eq. (1). Note that the frequency shift is zero when the standard acoustic path with $\tilde{\theta} = \Theta$ is followed.

References

[1] Sijtsma, P., Oerlemans, S., Tibbe, T., Berkefeld, T. and Spehr, C. "Spectral Broadening by Shear Layers of Open Jet Wind Tunnels," AIAA 2014-3178, 2014, 20th AIAA/CEAS Aeroacoustics Conference, Atlanta, GA, June 16–20.

[2] Kröber, S., Hellmold, M. and Koop, L. "Experimental Investigation of Spectral Broadening of Sound Waves by Wind Tunnel Shear Layers," AIAA 2013-2255, 19th AIAA/CEAS Aeroacoustics Conference, Berlin, Germany, May 27–29.

[3] Cargill, A.M. "Sound Propagation through Fluctuating Flows – Its Significance in Aeroacoustics," AIAA Paper 83-697, 1983.

[4] Powles, C.J., Tester, B.J. and McAlpine, A. "A Weak Scattering Model for Turbine-Tone Haystacking Outside the Cone of Silence", International Journal of Aeroacoustics, Vol. 10, Nr. 1, 2011, pp. 17-50.

[5] McAlpine, A., Powles, C.J. and Tester, B.J. "A Weak Scattering Model for Tone Haystacking," AIAA Paper 2009-3216, 15th AIAA/CEAS Aeroacoustics Conference, Miami, FL, 11-13 May.

[6] Sijtsma, P. "CLEAN Based on Spatial Source Coherence", International Journal of Aeroacoustics, Vol. 6, No. 4, 2007, pp. 357-374.

[7] Schlinker, R.H. and Amiet, R.K., "Refraction and Scattering of Sound by A Shear Layer", AIAA 80-0973, 1980, 6th AIAA Aeroacoustics Conference, Hartford, CT, June 4–6.